

A Switching Median Filter With Boundary Discriminative Noise Detection for Extremely Corrupted Images

Pei-Eng Ng and Kai-Kuang Ma, *Senior Member, IEEE*

Abstract—A novel switching median filter incorporating with a powerful impulse noise detection method, called the *boundary discriminative noise detection* (BDND), is proposed in this paper for effectively denoising extremely corrupted images. To determine whether the current pixel is corrupted, the proposed BDND algorithm first classifies the pixels of a localized window, centering on the current pixel, into three groups—*lower intensity impulse noise*, *uncorrupted pixels*, and *higher intensity impulse noise*. The center pixel will then be considered as “uncorrupted,” provided that it belongs to the “uncorrupted” pixel group, or “corrupted.” For that, two boundaries that discriminate these three groups require to be accurately determined for yielding a very high noise detection accuracy—in our case, achieving zero miss-detection rate while maintaining a fairly low false-alarm rate, even up to 70% noise corruption. Four noise models are considered for performance evaluation. Extensive simulation results conducted on both monochrome and color images under a wide range (from 10% to 90%) of noise corruption clearly show that our proposed switching median filter substantially outperforms all existing median-based filters, in terms of suppressing impulse noise while preserving image details, and yet, the proposed BDND is algorithmically simple, suitable for real-time implementation and application.

Index Terms—Image denoising, impulse noise detection, nonlinear filter, switching median filter.

I. INTRODUCTION

DIGITAL images could be contaminated by impulse noise during image acquisition or transmission. The intensity of impulse noise has the tendency of being either relatively high or relatively low. Thus, it could severely degrade the image quality and cause some loss of information details. Various filtering techniques have been proposed for removing impulse noise in the past, and it is well-known that linear filters could produce serious image blurring. As a result, nonlinear filters have been widely exploited due to their much improved filtering performance, in terms of impulse noise attenuation

and edge/details preservation. One of the most popular and robust nonlinear filters is the *standard median* (SM) filter [1], which exploits the rank-order information of pixel intensities within a filtering window and replaces the center pixel with the median value. Due to its effectiveness in noise suppression and simplicity in implementation, various modifications of the SM filter have been introduced, such as the *weighted median* (WM) [2] filter and the *center weighted median* (CWM) [3] filter.

Conventional median filtering approaches apply the median operation to each pixel unconditionally, that is, without considering whether it is uncorrupted or corrupted. As a result, the image details contributed from the uncorrupted pixels are still subject to be filtered, and this causes image quality degradation. An intuitive solution to overcome this problem is to implement an impulse-noise detection mechanism prior to filtering; hence, only those pixels identified as “corrupted” would undergo the filtering process, while those identified as “uncorrupted” would remain intact. By incorporating such noise detection mechanism or “intelligence” into the median filtering framework, the so-called *switching median filters* [4]–[11] had shown significant performance improvement.

Early-developed switching median filters are commonly found being nonadaptive to a given, but unknown, noise density and prone to yielding pixel misclassifications especially at higher noise density interference. To address this issue, the *noise adaptive soft-switching median* (NASM) filter was proposed in [9], which consists of a three-level hierarchical soft-switching noise detection process. The NASM achieves a fairly robust performance in removing impulse noise, while preserving signal details across a wide range of noise densities, ranging from 10% to 50%. However, for those corrupted images with noise density greater than 50%, the quality of the recovered images become significantly degraded, due to the sharply increased number of misclassified pixels.

In this paper, we propose a highly-accurate noise detection algorithm, called the *boundary discriminative noise detection* (BDND), which can handle image corruption even up to 90% noise density. Together with the modified NASM median filtering scheme, the proposed BDND has shown far superior performance in terms of subjective quality in the filtered image as well as objective quality in the *peak signal-to-noise ratio* (PSNR) measurement to that of the NASM filter. For denoising color images, our proposed BDND filter consistently shows impressive results as well.

The paper is divided into five sections as follows. Section II introduces our proposed BDND algorithm for impulse noise

Manuscript received March 4, 2005; revised June 6, 2005. The associate editor coordinating the review of this manuscript and approving it for publication was Dr. Ron Kimmel.

P.-E. Ng was with the School of Electrical and Electronic Engineering, Nanyang Technological University, Singapore 639798. She is now with HealthSTATS International Pte., Ltd., Singapore 536199 (e-mail: peng@healthstats.com.sg).

K.-K. Ma is with the School of Electrical and Electronic Engineering, Nanyang Technological University, Singapore 639798 (e-mail: ekkma@ntu.edu.sg).

Digital Object Identifier 10.1109/TIP.2005.871129

identification. Section III describes the filtering scheme in response to the noise detection results. Section IV presents extensive simulation results. Section V concludes this paper.

II. IMPULSE-NOISE DETECTION

A. Noise Models

Four impulse noise models are implemented, for extensively examining the performance of our proposed filter with consideration of practical situations. Each model is described in detail as follows.

1) *Noise Model 1:* Noise is modeled as salt-and-pepper impulse noise as practiced (e.g., in [9]). Pixels are randomly corrupted by two fixed extremal values, 0 and 255 (for 8-bit monochrome image), generated with the same probability. That is, for each image pixel at location (i, j) with intensity value $s_{i,j}$, the corresponding pixel of the noisy image will be $x_{i,j}$, in which the probability density function of $x_{i,j}$ is

$$f(x) = \begin{cases} \frac{p}{2}, & \text{for } x = 0 \\ 1 - p, & \text{for } x = s_{i,j} \\ \frac{p}{2}, & \text{for } x = 255 \end{cases} \quad [\text{Model 1}]$$

where p is the noise density.

2) *Noise Model 2:* For the Model 2, it is similar to Model 1, except that each pixel might be corrupted by either “pepper” noise (i.e., 0) or “salt” noise with *unequal* probabilities. That is

$$f(x) = \begin{cases} \frac{p_1}{2}, & \text{for } x = 0 \\ 1 - p, & \text{for } x = s_{i,j} \\ \frac{p_2}{2}, & \text{for } x = 255 \end{cases} \quad [\text{Model 2}]$$

where $p = p_1 + p_2$ is the noise density and $p_1 \neq p_2$.

3) *Noise Model 3:* Instead of two fixed *values*, impulse noise could be more realistically modeled by two fixed *ranges* that appear at both ends with a length of m each, respectively. For example, if m is 10, noise will equal likely be any values in the range of either [0, 9] or [246, 255]. That is

$$f(x) = \begin{cases} \frac{p}{2m}, & \text{for } 0 \leq x < m \\ 1 - p, & \text{for } x = s_{i,j} \\ \frac{p}{2m}, & \text{for } 255 - m < x \leq 255 \end{cases} \quad [\text{Model 3}]$$

where p is the noise density.

4) *Noise Model 4:* Model 4 is similar to Model 3, except that the densities of low-intensity impulse noise and high-intensity impulse noise are *unequal*. That is

$$f(x) = \begin{cases} \frac{p_1}{m}, & \text{for } 0 \leq x < m \\ 1 - p, & \text{for } x = s_{i,j} \\ \frac{p_2}{m}, & \text{for } 255 - m < x \leq 255 \end{cases} \quad [\text{Model 4}]$$

where $p = p_1 + p_2$ is the noise density and $p_1 \neq p_2$.

B. Noise Detection

The proposed BDND algorithm is applied to each pixel of the noisy image in order to identify whether it is “uncorrupted” or “corrupted.” After such an application to the entire image, a two-dimensional binary decision map is formed at the end

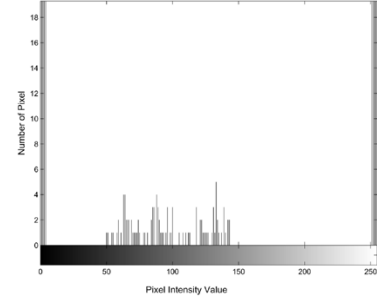


Fig. 1. Histogram distribution of 21×21 subimage of “Lena” corrupted by 80% impulse noise.

of the noise detection stage, with “0s” indicating the positions of “uncorrupted” pixels, and “1s” for those “corrupted” ones. To accomplish this objective, all the pixels within a pre-defined window that center around the considered pixel will be grouped into three clusters; hence, two boundaries b_1 and b_2 are required to be determined. For each pixel $x_{i,j}$ being considered, if $0 \leq x_{i,j} \leq b_1$, the pixel will be assigned to the *lower*-intensity cluster; otherwise, to the *medium*-intensity cluster for $b_1 < x_{i,j} \leq b_2$ or to the *high*-intensity cluster for $b_2 < x_{i,j} \leq 255$.

Obviously, if the center pixel being considered falls onto the middle cluster, it will be treated as “uncorrupted,” since its intensity value is neither relatively low nor relatively high. Otherwise, it is very likely that the pixel has been corrupted by impulse noise. Clearly, the accuracy of clustering results (hence, the accuracy of noise detection) ultimately depends on how accurate the identified boundaries b_1 and b_2 are.

First, we shed the light of our intuition that leads to the development of the proposed BDND algorithm simply based on the histogram distribution of a 21×21 subimage (Fig. 1) extracted from the simulated noisy image “Lena” corrupted by 80% impulse noise density based on the above-mentioned Noise Model 3. For illustrating a “typical” histogram distribution, the subimage chosen bears a “neutral” image content, meaning that the content is neither too “flat” (containing low frequency) nor too “busy” (containing high frequency). It could be observed that the distribution presented at the two ends of the distribution are most likely contributed by impulse noise. Furthermore, the locations of two distinct gaps (or valleys) mark the most possible positions of the two boundaries, respectively, that clearly separate the impulse noise regions (at the two ends) from the uncorrupted pixel region (a much wider region in between); thus, dividing all the pixels within the window into three groups—the lower intensity impulse noise, the uncorrupted pixels (in the middle) and the higher intensity impulse noise.

The proposed *boundary discriminative* process consists of two iterations, in which the second iteration will only be invoked conditionally. In the first iteration, an enlarged local window with a size of 21×21 (empirically determined) is used to examine whether the considered pixel is an uncorrupted one. If the pixel fails to meet the condition to be classified as “uncorrupted” (i.e., not falling onto the middle cluster), the second iteration will be invoked to further examine the pixel based on a more confined local statistics by using a 3×3 window. In summary, the steps of the proposed BDND are:

- Step 1) Impose a 21×21 window, which is centered around the current pixel.
- Step 2) Sort the pixels in the window according to the ascending order and find the median, med , of the sorted vector \mathbf{v}_o .
- Step 3) Compute the intensity difference between each pair of adjacent pixels across the sorted vector \mathbf{v}_o and obtain the difference vector \mathbf{v}_D .
- Step 4) For the pixel intensities between 0 and med in the \mathbf{v}_o , find the maximum intensity difference in the \mathbf{v}_D of the same range and mark its corresponding pixel in the \mathbf{v}_o as the boundary b_1 .
- Step 5) Likewise, the boundary b_2 is identified for pixel intensities between med and 255; three clusters are, thus, formed.
- Step 6) If the pixel belongs to the middle cluster, it is classified as “uncorrupted” pixel, and the classification process stops; else, the second iteration will be invoked in the following.
- Step 7) Impose a 3×3 window, being centered around the concerned pixel and repeat Steps 2)–5).
- Step 8) If the pixel under consideration belongs to the middle cluster, it is classified as “uncorrupted” pixel; otherwise, “corrupted.”

For the understanding of the algorithmic steps mentioned above, a 5×5 (instead of 21×21) windowed subimage with the center pixel “202” (being boxed) is used as an example for illustrating the proposed BDND process as follows:

$$\mathbf{W} = \begin{pmatrix} 255 & 255 & 47 & 255 & 39 \\ 50 & 255 & 255 & 0 & 0 \\ 0 & 0 & 202 & 224 & 205 \\ 62 & 255 & 0 & 0 & 255 \\ 255 & 72 & 81 & 0 & 179 \end{pmatrix}.$$

- Pixel intensities are sorted in the ascending order and represented as a vector, where the median med is 81; i.e., $\mathbf{v}_o = [0\ 0\ 0\ 0\ 0\ 0\ 0\ 39\ 47\ 50\ 62\ 72\ 81\ 179\ 202\ 205\ 224\ 255\ 255\ 255\ 255\ 255\ 255]$.
- The vector of intensity differences between each pair of two adjacent pixels in \mathbf{v}_o is computed as: $\mathbf{v}_D = [0\ 0\ 0\ 0\ 0\ 0\ 39\ 8\ 3\ 12\ 10\ 9\ 98\ 23\ 3\ 22\ 31\ 0\ 0\ 0\ 0\ 0\ 0\ 0]$.
- For the pixels with intensities between 0 and med in the \mathbf{v}_o , the corresponding maximum difference in the \mathbf{v}_D is 39, which is the difference between the pixel intensities 0 and 39.
- For the pixels with intensities between med and 255 in the \mathbf{v}_o , the maximum difference in the \mathbf{v}_D is 98, which is the difference between the pixel intensities 81 and 179.
- Hence, $b_1 = 0$ and $b_2 = 81$. Thus, the lower intensity cluster is $\{0, 0, 0, 0, 0, 0, 0\}$, the medium-intensity cluster is $\{39, 47, 50, 62, 72, 81\}$, and the higher intensity cluster is $\{179, 202, 205, 224, 255, 255, 255, 255, 255, 255, 255\}$.

TABLE I
SUGGESTED WINDOW SIZE FOR THE ESTIMATED NOISE DENSITY LEVEL p

Noise Density	$W_{D1} \times W_{D1}$
$0\% < p \leq 20\%$	3×3
$20\% < p \leq 40\%$	5×5
$> 40\%$	7×7

- Since the center pixel “202” belongs to the higher intensity cluster, hence, the second iteration needs to be invoked, and a 3×3 window is imposed and centered around it

$$\mathbf{W}_{3 \times 3} = \begin{pmatrix} 255 & 255 & 0 \\ 0 & 202 & 224 \\ 255 & 0 & 0 \end{pmatrix}.$$

- Now, the pixel intensities are sorted and represented in the vector form: $\mathbf{v}_o = [0\ 0\ 0\ 0\ 202\ 224\ 255\ 255\ 255]$.
- As before, the vector of intensity differences is computed: $\mathbf{v}_D = [0\ 0\ 0\ 202\ 22\ 31\ 0\ 0]$.
- The first maximum difference is 202, which is the difference between the pixel intensities 0 and 202. The second maximum difference is 31, which is the difference between the pixel intensities 224 and 255.
- Hence, $b_1 = 0$ and $b_2 = 224$. Thus, the lower intensity cluster is $\{0, 0, 0, 0\}$, the medium-intensity cluster is $\{202, 224\}$, and the higher intensity cluster is $\{255, 255, 255\}$.
- At the end of the discrimination process, the center pixel “202” is classified as an “uncorrupted” pixel, since it belongs to the middle cluster.

C. Color Image Noise Detection

As the most directly used color space for digital image processing, the RGB color space is chosen in our work to represent the color images. In the RGB color space, each pixel at the location (i, j) can be represented as color vector $s_{i,j} = (s_{i,j}^R, s_{i,j}^G, s_{i,j}^B)$, where $s_{i,j}^R$, $s_{i,j}^G$, and $s_{i,j}^B$ are the red (R), green (G), and blue (B) components, respectively. The noisy color images are modeled by injecting the salt-and-pepper noise randomly and independently to each of these color components. That is, when a color image is being corrupted by the noise density p , it means that each color component is being corrupted by p . Thus, for each pixel $s_{i,j}$, the corresponding pixel of the noisy image will be denoted as $x_{i,j} = (x_{i,j}^R, x_{i,j}^G, x_{i,j}^B)$, in which the probability density functions of each color components can be one of the noise models described earlier. In this work, Noise Model 1 is used for performance demonstration.

The process of extending the noise detection algorithm to corrupted color images is straightforward. The proposed BDND algorithm will be simply applied to R-, G-, and B-planes individually, and three binary decision maps are obtained.

III. NOISE-ADAPTIVE FILTERING

Although the major contributions of making the entire switching median filter being *noise-adaptive* come from the impulse-noise detection as described in the previous section,



Fig. 2. First column shows three original test images: (top) “Lena,” (middle) “Peppers,” and (bottom) “Baboon,” and the second column presents their corresponding noisy images with 80% impulse noise corruption generated by Noise Model 1.

the post-detection filtering to be discussed in this section also contributes to the overall denoising performance. Based on the filtering process described in [9], in the follow-up two subsections, we shall highlight this aspect and provide three additional improvements on the filtering stage.

A. Simplified Noise-Density Estimation

In order to determine the window size of the filtering window $W_F \times W_F$, the limit of the maximum window size $W_{D1} \times W_{D1}$ requires to be determined first. For that, Table I is empirically established based on multiple test images, in which different window sizes are suggested for different noise-density levels of corruption estimated. To conduct the estimation of noise density, NASM involves a set of sophisticated procedures (such as quad-tree decomposition) [9]. On the contrary, the noise-density

estimation performed in the proposed BDND is much simpler, simply by counting the number of 1s on the binary decision map obtained in the impulse-noise detection stage conducted earlier.

Based on the binary decision map, “*no filtering*” is applied to those “uncorrupted” pixels, while the SM filter with an adaptively determined window size $W_F \times W_F$ is applied to each “corrupted” one.¹

B. Algorithmic Improvement on Filtering

Compare with the NASM’s filtering stage, there are three changes (in italic for the ease of identification) for further performance improvement as described in the following.

¹Recall that in the NASM [9], the decision map contains three categories yielded in the noise detection stage—the “true pixel,” the “noisy pixel,” and the “edge pixel.” They are treated by “*no filtering*,” the SM filtering, and a fuzzy-weighted median filtering, respectively, in the filtering stage.

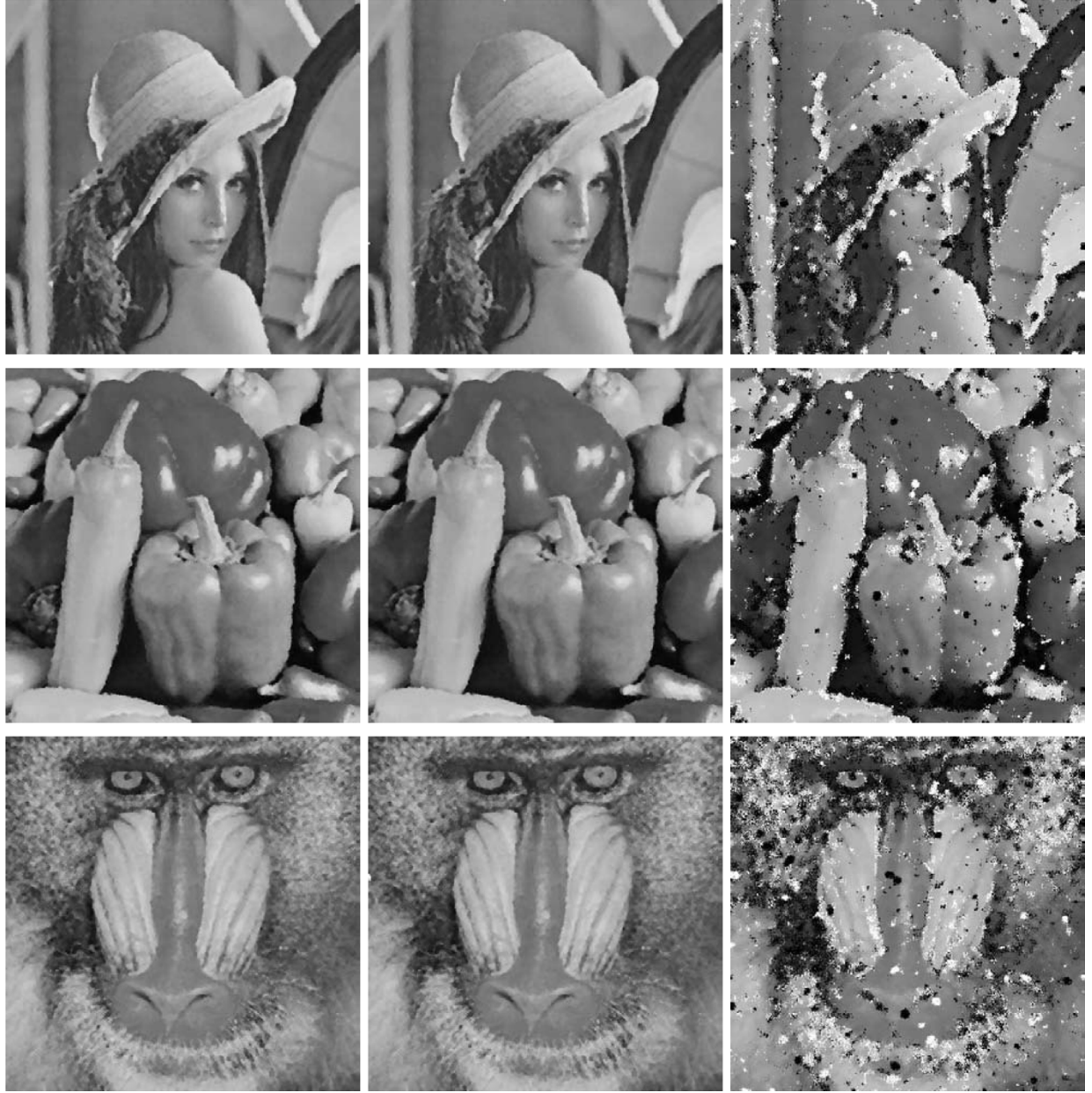


Fig. 3. Results of denoising corrupted images “Lena,” “Peppers,” and “Baboon” (with 80% impulse noise density) in Fig. 2 by using the ideal switching filter (first column), the proposed switching median filter with the BDND incorporated (second column), and the NASM filter (third column), respectively.

First, the maximum window size $W_{D1} \times W_{D1}$ is limited to 7×7 (instead of 11×11 as suggested in [9]) in order to avoid severe blurring of image details at high noise density cases (i.e., $p > 50\%$). After that, the filter’s window size $W_F \times W_F$ is obtained in a similar way as that proposed in [9] with a slight modification as follows.

In the NASM [9], starting with $W_F = 3$, the filtering window iteratively extends outward by one pixel in all the four sides of the window, provided that the number of uncorrupted pixels (denoted by N_c) is less than half of the total number of pixels (denoted by $S_{in} = (1/2)[W_F \times W_F]$) within the filtering window, while $W_F \leq W_{D1}$. In this work, an additional condition is further imposed, such that the filtering window will also be extended when the number of uncorrupted pixels is equal to zero. Therefore, the second change for improvement is that while

($N_c < S_{in}$ and $W_F \leq W_{D1}$) or ($N_c = 0$), window $W_F \times W_F$ will be extended by one pixel outward in all the four sides of the window.

By exploiting the SM filter with the window size of $W_F \times W_F$ to a noise pixel, the output pixel Y_{ij} is

$$Y_{ij} = \text{median}\{X_{i-s,j-t} | (s,t) \in W\}$$

where $W = \{(s,t) | -(W_F - 1)/2 \leq s, t \leq (W_F - 1)/2\}$. In [9], the current pixel is included in the filtering (ranking) process. Note that the current pixel has already been identified as “corrupted;” thus, our third change in the proposed BDND is to exclude the current pixel in the process of filtering; that is, only those “uncorrupted” pixels within the window W are considered for the process of ranking. This will, in turn, yield a better filtering result with less distortion.

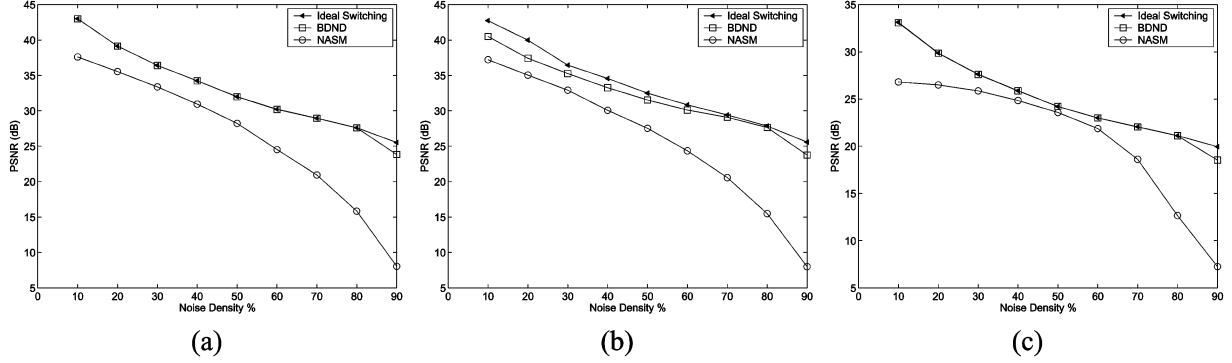


Fig. 4. PSNR performance comparison of using the ideal switching filter, the proposed switching median filter with the BDND incorporated, and the NASM filter on: (a) “Lena;” (b) “Peppers;” and (c) “Baboon,” corrupted by various noise densities.

C. Color Image Denoising

The switching median filtering scheme can be extended to denoise corrupted color images via the *scalar median* filtering approach as well as the *vector median* filtering approach. The scalar approach treats each color component as an independent entity; that is, the same filtering scheme will be applied to R-, G-, and B-planes independently, as if each plane is a separate monochrome image. The filtered R-, G-, and B-planes will be then combined to form the recovered color image.

The vector median filtering approach treats each pixel as a vector rather than three separate components on the filtering stage; thus, the three binary decision maps obtained from the noise-detection stage are combined into a binary decision map (through the logical “OR” function) to mark the locations of “corrupted” pixels; that is, the current pixel will be considered as “corrupted,” if at least one of its components is detected as “corrupted.” The size of the filtering window centered around each “corrupted” pixel to be filtered is adaptively determined by following the same procedures as the filtering process conducted for the monochrome images. Only those uncorrupted pixels within the window are taken into account on computing the median vector, for replacing the considered (corrupted) pixel located at the center of the window. For a set of uncorrupted pixel vectors $\{\mathbf{x}_1, \dots, \mathbf{x}_n\}$, the steps of computing the median pixel are as follows [14]. 1) For each pixel vector \mathbf{x}_i , compute its L_1 -norm distances with respect to other pixel vectors \mathbf{x}_j individually and sum them together. That is, $S_i = \sum_{j=1}^N \|\mathbf{x}_i - \mathbf{x}_j\|$, for $i = 1, \dots, N$. 2) Find the S_{\min} which is the minimum of all S_i (for $i = 1, \dots, N$), and the vector median \mathbf{x}_{\min} corresponds to the \mathbf{x}_i that yields S_{\min} .

IV. SIMULATION RESULTS

A. Monochrome Images

The performance evaluation of the filtering operation is quantified by the PSNR calculated using the following standard formula:

$$\text{PSNR} = 10 \log_{10} \left(\frac{255^2}{\text{MSE}} \right) \text{ dB}$$

and

$$\text{MSE} = \frac{1}{MN} \sum_{i=1}^M \sum_{j=1}^N (y_{i,j} - s_{i,j})^2$$

where M and N are the total number of pixels in the horizontal and the vertical dimensions of the image; $s_{i,j}$ and $y_{i,j}$ denote the original and filtered image pixels, respectively.

1) *Based on Noise Model 1:* Intensive simulations were carried out using several monochrome images, from which “Lena,” “Peppers,” and “Baboon” are chosen for demonstrations in Fig. 2, whereby the original images (left column) and their corrupted versions with 80% noise density injected (right column) are shown side by side. The filtering performance of the *ideal switching* filter, the proposed switching median filter with the BDND incorporated and the NASM filter are documented in Fig. 3 for comparison. The ideal switching filter is realized by incorporating the ideal noise detection, which is based on the *perfect* binary decision map generated by recording the exact position of each injected impulse noise during the simulation of noisy image. Using the perfect binary decision map incorporated with our filtering scheme as stated in Section III, the performance of the ideal switching filter is served as the benchmark in our comparisons. It could be obviously observed from Fig. 3 that, for such a high corruption level (i.e., 80%), our results are far superior to that of the NASM filter. The recovered images using the NASM filter, although still comprehensible in overall image contents, are degraded by a significant amount of noticeable noise blotches.

Fig. 4 graphically illustrates the quantitative performance comparison in terms of PSNR measurements. Consistently, our results outperform that of the NASM filter across a wide range of noise densities, and almost coincided with that of the ideal switching filter in multiple cases. On the contrary, the PSNR performance of the NASM filter starts to drop dramatically at noise density level 60% and onwards. This is mainly due to the large number of misclassified pixels incurred at these corruption levels. As for our proposed BDND approach, the PSNR is slightly and gradually degraded, since the decline is mainly contributed from more blurring when more pixels are identified as noise and filtered.

Since the noise detection plays the key role on denoising, it would be insightful to evaluate the performance purely contributed from that part, in terms of the number of *miss detection* (MD)—impulse noise being misdetected, and that of *false alarm* (FA)—uncorrupted pixel being misclassified as noise. For that, the binary maps obtained from applying the proposed BDND and NASMs noise detection algorithms to noisy image respec-

TABLE II

NUMBERS OF MD AND FA RESULTED AFTER APPLYING THE BDND AND NASM's NOISE DETECTION ALGORITHM INDIVIDUALLY TO NOISY IMAGES (A) "LENA," (B) "PEPPERS," AND (C) "BABOON" CORRUPTED UNDER VARIOUS NOISE DENSITIES

Noise %	Miss Detection (MD)		False Alarm (FA)	
	Proposed	NASM	Proposed	NASM
10	0	61	0	2743
20	0	142	2	754
30	0	369	1	435
40	0	861	5	271
50	0	2032	7	177
60	0	4643	6	130
70	0	11231	10	92
80	21	35016	10	403
90	190	124926	5	2608

(a)

Noise %	Miss Detection (MD)		False Alarm (FA)	
	Proposed	NASM	Proposed	NASM
10	0	111	353	2745
20	0	247	370	895
30	0	562	365	550
40	0	965	370	484
50	0	1559	282	360
60	0	2529	290	308
70	0	4803	260	197
80	12	11784	127	451
90	51	52286	336	2732

(b)

Noise %	Miss Detection (MD)		False Alarm (FA)	
	Proposed	NASM	Proposed	NASM
10	0	4	21	10007
20	0	18	30	5043
30	0	53	24	2708
40	0	66	29	1374
50	0	256	18	653
60	0	323	24	569
70	0	2429	18	133
80	6	11601	21	378
90	272	53770	16	3070

(c)

TABLE III

PSNR PERFORMANCE OF THE PROPOSED SWITCHING MEDIAN FILTER WITH THE BDND INCORPORATED ON TEST IMAGE LENA BEING CORRUPTED BY A TOTAL NOISE DENSITY OF (A) 70% AND (B) 80%, BUT COMPRISED OF DIFFERENT DENSITIES OF "SALT" AND "PEPPER" NOISE

Noise Density (%)		PSNR (dB)
Pepper (i.e., 0)	Salt (i.e., 255)	
20	50	14.1962
25	45	28.4459
30	40	28.9049
35	35	28.8562
40	30	28.9178
45	25	28.5729
50	20	8.7169

(a)

Noise Density (%)		PSNR (dB)
Pepper (i.e., 0)	Salt (i.e., 255)	
30	50	13.6390
35	45	27.0356
40	40	27.5541
45	35	27.2153
50	30	8.7169

(b)

TABLE IV
PSNR PERFORMANCE OF THE NASM FILTER AND THE PROPOSED SWITCHING MEDIAN FILTER WITH THE BDND INCORPORATED ON TEST IMAGE LENA BEING CORRUPTED BY A TOTAL NOISE DENSITY OF 80%, IN WHICH THE PERMISSIBLE RANGE OF BOTH LOW-INTENSITY AND HIGH-INTENSITY IMPULSE NOISE ARE DIFFERENT FOR EACH CASE

Noise Range		PSNR (dB)	
Low-intensity Impulse	High-intensity Impulse	NASM	BDND
[0, 9]	[246, 255]	15.4824	18.7889
[0, 19]	[236, 255]	15.8167	19.1385
[0, 29]	[226, 255]	16.1534	19.0744
[0, 39]	[216, 255]	16.4852	18.1270
[0, 49]	[206, 255]	16.9436	17.3103
[0, 59]	[196, 255]	17.2730	16.8712
[0, 69]	[186, 255]	17.6570	16.4657
[0, 79]	[176, 255]	17.8128	16.1372
[0, 89]	[166, 255]	17.9226	15.9073
[0, 99]	[156, 255]	17.4723	15.7174
[0, 109]	[146, 255]	16.4373	15.4173
[0, 119]	[136, 255]	16.0791	14.9509
	[0, 255]	15.8124	12.8406

tively are computed against the *perfect* binary decision maps mentioned earlier. As noted in Table II, our BDND algorithm impressively achieves zero MD rate even up to 70% noise density while maintaining a fairly low FA rate. On the other hand, a significant amount of both MD and FA are yielded by the NASMs method, especially at high noise densities. This accounts for the large performance gain of the proposed BDND filter against that of the NASM filter.

2) *Based on Model 2:* Experiments had been carried out for 70% and 80% corruption cases using test image Lena, each of which comprised of different densities (probabilities of occurrences) of "pepper" (i.e., 0) and "salt" (i.e., 255), according to Noise Model 2 as stated in Section II, and the results are shown in Table III. It could be observed that the proposed BDND algorithm still works quite well for unequal densities of "salt" and

TABLE V
PSNR PERFORMANCE OF THE PROPOSED SWITCHING MEDIAN FILTER WITH THE BDND INCORPORATED ON TEST IMAGE LENA BEING CORRUPTED WITH A TOTAL NOISE DENSITY OF 80%. THE PERMISSIBLE RANGE OF IMPULSE NOISE ARE $\{[0,29], [226,255]\}$ IN (A) AND $\{[0,39], [216,255]\}$ IN (B), RESPECTIVELY, FOR WHICH THE DENSITIES OF LOW-INTENSITY AND HIGH-INTENSITY IMPULSE NOISE ARE DIFFERENT IN EACH CASE

Noise Density (%)		PSNR (dB)
Low-intensity Impulse Noise	High-intensity Impulse Noise	
30	50	7.3172
35	45	17.6832
45	35	17.9835
50	30	6.2572

(a)

Noise Density (%)		PSNR (dB)
Low-intensity Impulse Noise	High-intensity Impulse Noise	
30	50	9.7040
35	45	16.8886
45	35	16.8766
50	30	10.3974

(b)



Fig. 5. (a) Original color image "Lena." (b) Noisy image "Lena" corrupted with 50% noise density on each color component. (Color version available online at <http://ieeexplore.ieee.org/>.)

"pepper" noise, provided that neither the density of "salt" nor that of "pepper" is equal to or more than 50%. The later is due to the fact that, the proposed BDND algorithm depends on the median of the windowed pixels as the first key step, and the computed median is quite likely a noise in these cases.

3) *Based on Model 3:* Table IV outlines the results of several experiments for the 80% corruption case, (using test image Lena). Starting off with impulse noise within the range of $\{[0,9], [246,255]\}$, the corruption range of both low-intensity and high-intensity noise were increased by 10 in each of the subsequent experiments (i.e., $\{[0,19], [236,255]\}, \{[0,29], [266,255]\}, \dots, \{[0,119], [136,255]\}$, up to $\{[0,255]\}$). Note that the PSNR measurements of the BDND algorithm drops gradually as the range of impulsive noise variation increases.

4) *Based on Model 4:* Experiments had been carried out using test image Lena being corrupted with impulse noise in the intensity range of $\{[0,29], [226,255]\}$ and $\{[0,39], [216,255]\}$.

In each experiment, image is 80% corrupted with unequal densities of the low-intensity and the high-intensity impulse noise. As shown in Table V, the proposed BDND algorithm still works fairly well under this model, provided that neither of the noise is as dense as 50% or more. This is due to the same reason as explained in the Noise Model 2.

B. Color Images

It is well known that the human perception of the *color* differences mismatches the *numerical* differences yielded in the RGB color space. Therefore, the perceptually uniform color space CIELAB, standardized by the Commission Internationale de l'Eclairage (CIE), is more accurate for defining quantitative measurements of perceptual error between the two color vectors. For that, both images will undergo two consecutive transformations—from the RGB color space to the XYZ color space [17], and then from the XYZ color space to the CIELAB color space [18].

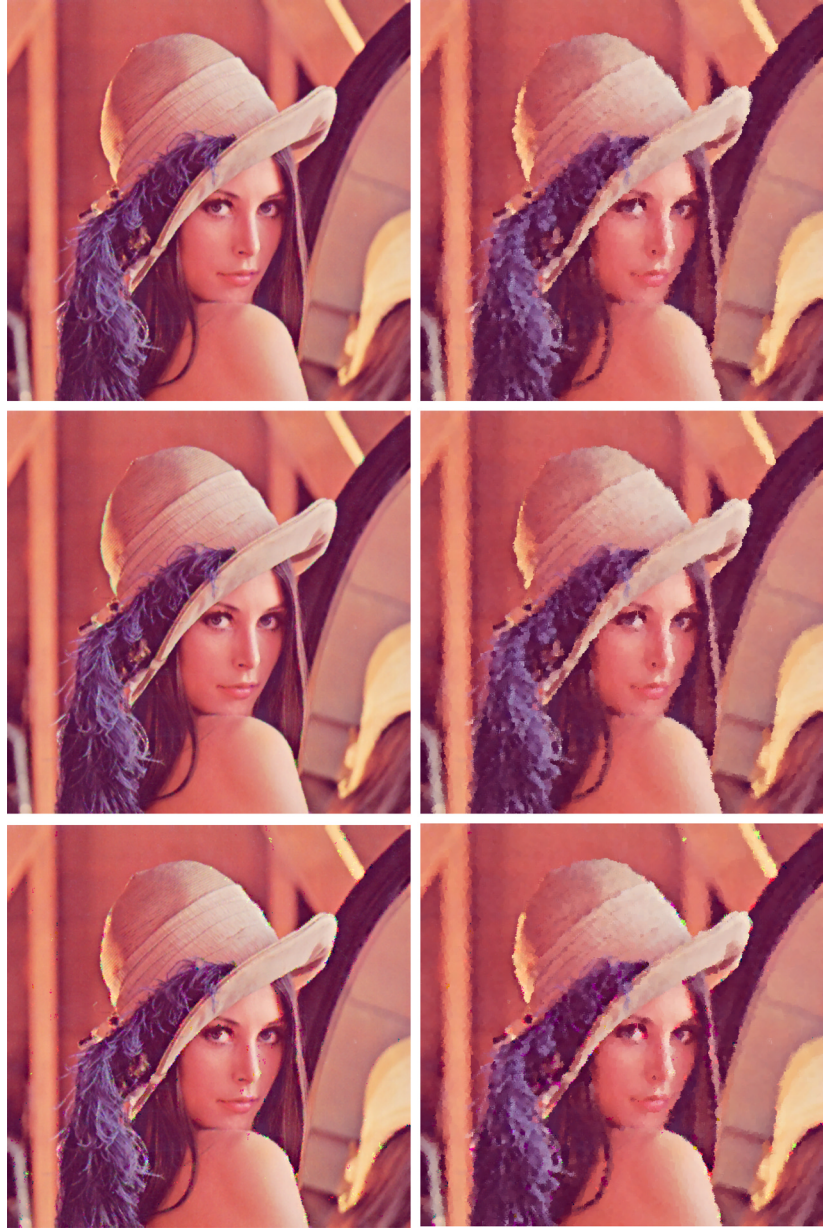


Fig. 6. Results of denoising corrupted color image “Lena” (with 50% impulse noise density on each color component image as based on the Noise Model 1) using the ideal switching filter (first row), the proposed switching median filter with the BDND incorporated (second row) and the NASM filter (third row), respectively. Each filter is implemented through the scalar–median filtering (left column) and *vector*–median filtering (right column) methodologies. (Color version available online at <http://ieeexplore.ieee.org>.)

In the CIELAB color space, the perceptually linear color difference formulas between two colors is [16]: $\Delta E_{ab}^* = \sqrt{(\Delta L^*)^2 + (\Delta a^*)^2 + (\Delta b^*)^2}$. Therefore, to measure the total difference between the recovered image and the original image (both recorded in the CIELAB space), the color difference ΔE_{ab}^* between each pair of two color samples of the two images is computed. All the differences ΔE_{ab}^* are then summed together across the entire image.

The original and noisy (corrupted by 50% noise density on each color component) color image “Lena” are depicted in Fig. 5. The noisy component images are separately treated by using the ideal switching filter, the proposed switching median filter with the BDND incorporated and the NASM filter, each being implemented via scalar and vector approaches. The

recovered images are shown in Fig. 6. Again, the performance of the NASM filter is much inferior to that of our proposed BDND filter, while ours is fairly close to that of the ideal switching filter. A more objective view could be observed from Fig. 7, whereby the quantitative color difference ΔE_{ab}^* measurements are plotted against various corruption levels. The proposed switching median filter with the BDND incorporated consistently yields impressive performance under a wide range of corruption from 10% to 70% noise densities.

Overall, the implementation of the switching median filters using the scalar approach resulted in less image quality degradation. In the vector median filtering approach, a pixel is considered as corrupted, as long as one of its components is detected as corrupted. Therefore, a higher noise density level will be re-

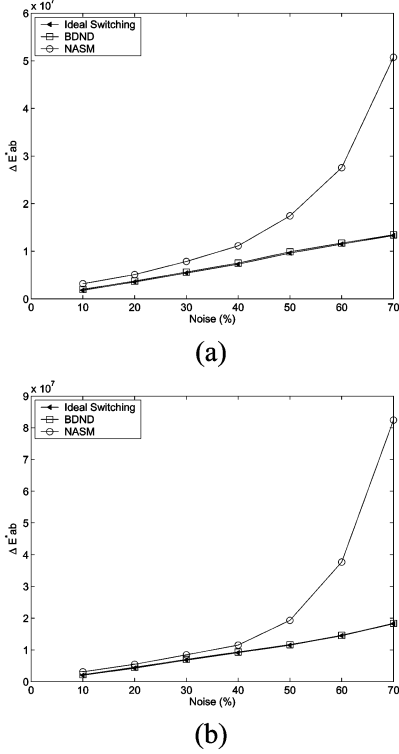


Fig. 7. Performance comparison of (top) scalar and (bottom) *vector* switching median filtering (test color image: “Lena”).

sulted, leading to a larger filtering window according to Section III. This in turn causes more blurs in its filtered image, and thus, higher color difference (error) measurement, as shown in Fig. 8.

V. CONCLUSION

In this paper, we proposed a novel, fairly accurate and simple impulse-noise detection method, called the BDND, which has been further incorporated into the framework of switching median filter as a very powerful image denoising scheme. Furthermore, improvements are also made in the noise-adaptive *filtering* stage as described in Section III-B. To consider possible variations often encountered in practical cases, four noise models are used to generate impulse noise. Extensive simulation results reveal that our filter consistently outperforms the NASM filter (especially, with a large margin of improvement at extremely high noise density corruption) by attaining much higher PSNR across a wide range of noise densities, from 10% to 90%. The key success of such performance delivery is mainly due to highly accurate noise detection accomplished by the BDND algorithm—achieving zero miss-detection rate up to 70% noise density corruption (based on Noise Model 1) while maintaining a fairly low false-alarm rate. Together with additional improvements contributed from the post-detection filtering stage, the entire switching median filtering performance has yielded a very close performance to that of the ideal-switching case consistently.

Another tremendous advantage of the proposed BDND algorithm is that it is fairly simple to implement for real-time image applications.

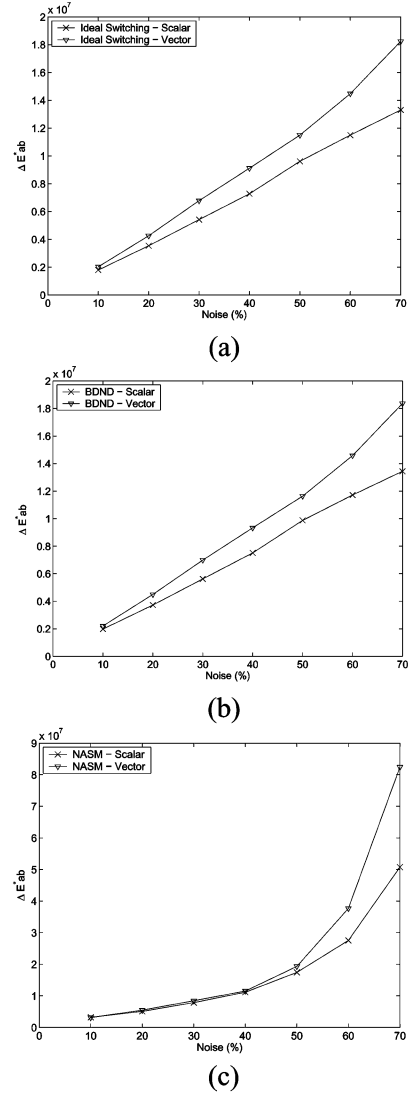


Fig. 8. Performance comparison between the two methodologies, *scalar* switching median and *vector* switching median filtering, using: (a) the ideal switching filter; (b) the proposed switching median filter with the BDND incorporated; and (c) the NASM filter. (Test color image: “Lena”).

REFERENCES

- [1] I. Pitas and A. N. Venetsanopoulos, “Order statistics in digital image processing,” *Proc. IEEE*, vol. 80, no. 12, pp. 1893–1921, Dec. 1992.
- [2] D. R. K. Brownrigg, “The weighted median filter,” *Commun. ACM*, vol. 27, no. 8, pp. 807–818, Aug. 1984.
- [3] S.-J. Ko and Y. H. Lee, “Center weighted median filters and their applications to image enhancement,” *IEEE Trans. Circuits Syst.*, vol. 38, no. 9, pp. 984–993, Sep. 1991.
- [4] T. Sun and Y. Neuvo, “Detail-preserving median based filters in image processing,” *Pattern Recognit. Lett.*, vol. 15, no. 4, pp. 341–347, Apr. 1994.
- [5] D. A. Florencio and R. W. Schafer, “Decision-based median filter using local signal statistics,” in *Proc. SPIE Vis. Commun. Image Process.*, vol. 2308, Sep. 1994, pp. 268–275.
- [6] T. Chen, K.-K. Ma, and L.-H. Chen, “Tri-state median filter for image denoising,” *IEEE Trans. Image Process.*, vol. 8, no. 12, pp. 1834–1838, Dec. 1999.
- [7] Z. Wang and D. Zhang, “Progressive switching median filter for the removal of impulse noise from highly corrupted images,” *IEEE Trans. Circuits Syst. II*, vol. 46, no. 1, pp. 78–80, Jan. 1999.
- [8] S. Zhang and M. A. Karim, “A new impulse detector for switching median filters,” *IEEE Signal Process. Lett.*, vol. 9, no. 4, pp. 360–363, Nov. 2002.

- [9] H.-L. Eng and K.-K. Ma, "Noise adaptive soft-switching median filter," *IEEE Trans. Image Process.*, vol. 10, no. 2, pp. 242–251, Feb. 2001.
- [10] G. Pok, J.-C. Liu, and A. S. Nair, "Selective removal of impulse noise based on homogeneity level information," *IEEE Trans. Image Processing*, vol. 12, no. 1, pp. 85–92, Jan. 2003.
- [11] H. Hwang and R. A. Haddad, "Adaptive median filters: New algorithms and results," *IEEE Trans. Image Process.*, vol. 4, no. 4, pp. 499–502, Apr. 1995.
- [12] M. Nikovla, "A variational approach to remove outliers and impulse noise," *J. Math. Imag. Vis.*, vol. 20, pp. 99–120, 2004.
- [13] C.-S. Lee, C.-Y. Hsu, and Y.-H. Kuo, "Intelligent fuzzy image filter for impulse noise removal," in *Proc. IEEE Int. Conf. Fuzzy Syst.*, vol. 1, May 2002, pp. 431–436.
- [14] J. Astola, P. Haavisto, and Y. Neuvo, "Vector median filters," *Proc. IEEE*, vol. 78, no. 4, pp. 678–689, Apr. 1990.
- [15] A. J. Bardos and S. J. Sangwine, "Selective vector median filtering of color images," in *Proc. Int. Conf. IPA*, vol. 2, Jul. 1997, pp. 708–711.
- [16] M. Tkalcic and J. F. Tasic, "Color spaces: Perceptual, historical and application background," in *Proc. IEEE EUROCON*, vol. 1, Sep. 2003, pp. 304–308.
- [17] W. K. Pratt, *Digital Image Processing*, 3rd ed. New York: Wiley, 2001.
- [18] C. Connolly and T. Fleiss, "A study of efficiency and accuracy in the transformation from RGB to CIELAB color spaces," *IEEE Trans. Image Process.*, vol. 6, no. 7, pp. 1046–1048, Jul. 1997.



Pei-Eng Ng received the B.Eng. degree (hons.) in electronics majoring in multimedia from Multimedia University, Malaysia, in 2001, and the M.Sc. degree in signal processing from Nanyang Technological University, Singapore, in 2005.

From October 2004 to October 2005, she was a Project Officer with the Centre for Signal Processing, School of Electrical and Electronic Engineering, Nanyang Technological University, Singapore. She is currently with HealthSTATS International Pte., Ltd., Singapore. Her research interests include image denoising and image retrievals.



Kai-Kuang Ma (S'80–M'84–SM'95) received the B.E. degree from Chung Yuan Christian University, Chung-Li, Taiwan, R.O.C., in electronic engineering, the M.S. degree from Duke University, Durham, NC, in electrical engineering, and the Ph.D. degree from North Carolina State University, Raleigh, in electrical engineering.

He is currently a Professor with the School of Electrical and Electronic Engineering, Nanyang Technological University, Singapore. Prior to that (1992 to 1995), he was a Member of Technical Staff at the Institute of Microelectronics, National University of Singapore, working on digital video coding and the MPEG standards. From 1984 to 1992, he was with IBM Corporation at Kingston, NY, and then Research Triangle Park, NC, engaging in various DSP and VLSI advanced product development. His research interests are in the areas of digital signal, image, and video processing. These include digital image/video coding and standards, wavelets and filter banks, joint source/channel image coding, denoising, error resilience and concealment, and content-based image/video indexing and retrieval. He has served as Singapore MPEG Chairman and Head of Delegation (1997 to 2001). On the MPEG contributions, two fast motion estimation algorithms (Diamond Search and MVFAST) produced from his research group have been adopted by the MPEG-4 standard, as the reference core technology for fast motion estimation. He is the General Chair of organizing a series of international standard meetings (MPEG and JPEG), JPEG2000, and MPEG-7 workshops held in Singapore (March 2001).

Dr. Ma is currently an Editor of the *IEEE TRANSACTIONS ON COMMUNICATIONS*, an Associate Editor of the *IEEE TRANSACTIONS ON MULTIMEDIA*, an Associate Editor of the *International Journal of Image and Graphics*, and an Associate Editor of the *Journal of Visual Communication and Image Representation*. He is an elected Technical Committee Member of the IEEE Signal Processing Society Image and Multidimensional Signal Processing (IMDSP) and the IEEE Communications Society Multimedia Communications Committee. He has served as Technical Program Committee member, reviewer, and Session Chair of multiple IEEE international conferences. He was the Technical Program Co-Chair of the IEEE International Conference on Image Processing (ICIP) 2004 and Chairman of IEEE Signal Processing Singapore Chapter (2000 to 2002).